

Spiral Zipper Manipulator for Aerial Grasping and Manipulation

Chao Liu, Abhraneel Bera, Thulani Tsabedze, Daniel Edgar, and Mark Yim

Abstract—This paper presents a novel manipulator for aerial vehicles to perform grasping and manipulation tasks. The goal is to design a low-cost, relatively light but strong manipulator with a large workspace and compact storage space that can be mounted on an unmanned aerial system. A novel design solution based on the Spiral Zipper, an expanding tube, combined with tether actuators is presented. A model of the system is introduced and the control method and pose estimator are developed and tested with some experiments showing the reliable performance of the overall system. An experiment with a self-sealing suction cup gripper demonstrates manipulation while mounted on the aerial vehicle frame.

I. INTRODUCTION

Aerial vehicles are gaining interest within not only the research community, but also within industries and the public. More applications have been developed owing to their flexibility in restricted, unknown and difficult-to-reach environments, including industrial inspection, monitoring, aerial video, exploring unknown environments and mining. These are all passive sensing tasks for aerial vehicles. The ability to interact with the environment is a significant barrier to extending aerial vehicle applications. There are two challenging problems for aerial vehicles interacting with their environment: 1. possessing the necessary precision to perform the work and 2. delivering large enough forces to the environment [1]. There has been some work on improving flight stability [2] [3] [4] showing that perching on structures such as walls and ceilings is a promising approach. To deliver large forces, two strategies can be used — utilizing independently vectored thrust on the aerial vehicle to decouple its attitude from force delivery and leveraging environmental forces [1].

Aerial vehicles have many advantages over wheeled or legged terrestrial robots. They usually have a larger workspace, faster speed and easier planning solutions. This is especially significant when doing tasks in an unknown environment where wheeled or legged robots may encounter rough or inaccessible terrain. Hence, endowing aerial vehicles with terrestrial robot grasping and manipulation capabilities can enable applications beyond simple sensing. There are several design challenges to aerial manipulation. Ideally the manipulator is as light as possible due to the limited payload of aerial vehicles. A related design challenge is the workspace provided by the robotic arm. Lighter

The authors are with GRASP Lab and Department of Mechanical Engineering and Applied Mechanics, University of Pennsylvania, Philadelphia, PA 19104, USA {chaoliu, beraa, yim}@seas.upenn.edu, thulanit@alumni.upenn.edu, d.edgar14@gmail.com. This work was supported by ARL on the Robotic Perception, Intelligence, and Dexterous Manipulation & Unique Mobility, Robotics CTA 2010.

arms tends to lead to smaller arms and workspace, yet a larger workspace enables more flexibility for the attitude of the vehicle relative to the manipulated object. A larger workspace usually requires larger components to construct the arm which makes the stabilization of the vehicle difficult and reduces the maneuverability of the vehicle.

This paper presents a novel design of a robotic arm for an aerial vehicle to execute grasping and manipulation tasks. This work, based on our previous work [5], shows a complete solution for the design of a low-cost, light-weight but powerful, accurate and reliable aerial robotic arm with very compact storage. The paper is organized as follows. Sec. II reviews relevant previous work. Sec. III introduces the details of the design requirements and our design solution, including the mechanical and electrical design. Sec. IV discusses the kinematics model as well as the control strategy, and how we estimate the pose of the arm. Experimental results are shown in Sec. V. Finally, Sec. VI talks about the conclusions.

II. RELATED WORK

Different types of grippers have been installed on aerial vehicles without using robotic arms [6] [7] [8] resulting in beak or claw-style grasping tightly coupled with the vehicle's attitude and position. Serial manipulators have been designed for different types of aerial vehicles [9] [10] [11] [12] [13] using DC motors or servo motors. These arms usually have difficulty in cluttered environments and result in complex collision avoidance problems because the linkage's elbow often sweeps out a volume that may collide with the environment even when the path of the end-effector or carried object does not [14] [15]. Furthermore, in order to increase the payload of these arms, more powerful motors and stronger linkages are needed resulting in more inertia and a highly off-center mass which makes the platform stabilization difficult and seriously undermines the vehicles' maneuverability [11].

It is difficult for an aerial vehicle to maintain its position in the air in the presence of disturbances and also difficult for serial manipulators to compensate for these errors. Some parallel manipulators are designed for aerial grasping and manipulation tasks. These arms are composed of a base, a moving platform and multiple extendable rigid links, like Delta structures [16] [17] [18] [19]. Parallel manipulators have advantages in overcoming the imperfections of an aerial vehicle's positioning capabilities. Since all motors can work together to move the legs and the moving platform, smaller motors are required and the overall weight can be reduced. However, these designs usually have a limited reachable workspace or very long rigid linkages are required resulting in a heavy arm with a large storage space.

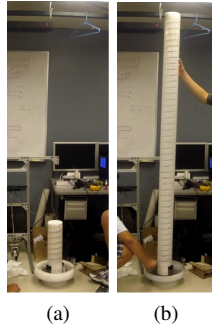


Fig. 1. The 57mm diameter Spiral Zipper starting to extend (a) and fully extended (b) [5].

A novel prismatic joint named *Spiral Zipper* (Fig. 1) is introduced in [5]. This joint is able to achieve a high extension ratio as well as form a high strength to weight ratio column to support large loads. A new robotic arm using a Spiral Zipper tube as well as three tether actuators named as a *tether-tube robot* is developed for aerial grasping and manipulation. Integrated with an active suction gripper, we have demonstrated wall grasping in the presence of positional noise by simulating experimental flight data from the aerial platform in [1]. The design details are shown, and the control and estimation method are presented in this work.

III. HARDWARE DESIGN

A. Requirements

The design constraints for this robotic system are set by the application it is intended for: flight on a large octorotor vehicle called the propulsion core capable of lifting well over 10 kilograms. Integration into that system comes with certain constraints dictated by the propulsion core's design team. First, a dual-arm system must be used. Second, a limit of 13.5 kg are to be allocated for use by the arm systems and payload. In the interest of providing room in the weight budget for an end-effector and whatever payload the arms manipulate, each arm subsystem must weigh less than 4.5 kg. In addition, each arm subsystem must be shaped to fit onto part of the octorotor's tube frame — an equilateral triangle 0.45 m each side. The arm needs to reach 1.5 m out yet collapse to less than 0.3 m and carry a payload of 1.8 kg.

The arm subsystem requires its own controller to convert desired poses from the octorotor system into motor commands, but in order to reduce the unbalancing weight of the arm on the edge of the frame, it is decided that power will come from the flyer's power supply system.

B. Mechanical Design

A Spiral Zipper tube is attached to a universal joint that is mounted onto a triangular base as shown in Fig. 2 and Fig. 2b. This is similar to an RRP manipulator with polar coordinate control axis. The end of the Spiral Zipper tube where an end-effector is placed is connected by three tethers. These three tethers control the two angular degrees-of-freedom (DOF) of the universal joint. The Spiral Zipper is the actuated prismatic DOF, so the system is overconstrained.

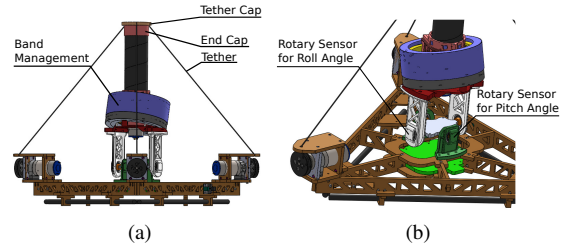


Fig. 2. (a) Manipulator Side View and (b) Universal Joint Close View

Fig. 2 show some key components of the manipulator. A bearing is mounted between the endcap and the tether attachment cap so that the motion of tether attachment cap is decoupled from the endcap as the Spiral Zipper spins. For most manipulation tasks, these three RRP DOF allow the end-effector to be positioned arbitrarily.

As described in [5], the Spiral Zipper actuator works best when under compression. The tethers clearly can only work under tension so, with the current configuration of tethers and the tube, they can work together to maintain their respective tension and compression states.

The ratio L/r , where L is the length of the column and r is the distance of the tether attachment point from the center of the column, determines how much force the column is applying to the base of the frame and consequently, how much torque the motors have to apply to reach a certain length. The goal is to minimize this ratio by making r as large as possible but at the same time not oversize it and make the system hard to integrate into the flyer. For this manipulator, the tether motors are placed as close as possible to the base's vertices at a distance of 23.5 cm from the center of the universal joint. Another concern when choosing motors is guaranteeing that even in the most difficult arm positions, it will still be able to manipulate a 1.8 kg object. But the motors are also potentially the heaviest piece of hardware on the arm, so balancing weight and torque is very important.

It is determined that the position which requires the most motor torque in the workspace involves the arm base positioned such that it is perpendicular to the ground with the arm pointed straight out parallel to the ground. The base is oriented so that one motor is high and two are low. In this configuration, all of the weight of the arm and its payload will be carried by a single motor at a position where the moment arm of that mass will be maximized for a given arm length.

At this maximum load scenario, it is found that the motor will have to handle at least 2.43 N m. To guarantee smooth operation at this limit case, three 165 rpm, 4.8 N m ServoCity DC motors are selected for the tether actuators. Each motor weighs 0.35 kg taking up a substantial portion of the manipulator's weight budget. There are more extreme loading scenarios possible should the arm approach the system's kinematic singularities but these are expressly ignored for design purposes under the assumption that the manipulator's path planning will navigate away from these positions.



Fig. 3. Spiral Zipper Manipulator Mounted on a 80/20 Frame

Due to the kinematics of the system, the main column is under considerably more load than the tethers at any given time. For example, in order to maintain its manipulability, all tethers must always remain tight. The geometry of the structure guarantees that a significant portion of the tension force from each tether is transmitted to the column. Any extension of the column needs to overcome not only inertial and friction forces inherent to zipper system, it also needs to overcome this necessary residual cable tension force. However, the zipper system is a natural screw, so the motor necessary to drive the system in this configuration doesn't need to be particularly powerful. Consequently, the 0.35 kg 165 rpm ServoCity motor used on the tether joints is also selected to drive the translation joint.

The base is laser cut out of a 6.35 mm MDF sheet, which is both low cost and low mass. A truss-like structure was implemented in order to achieve the structural strength required to maintain the internal forces from the system as well as the desired payload. The weight of the frame is 0.791 kg. The overall system is shown in Fig. 3.

The zipper system is structured to allow a maximum length of 1.5 m and a minimum retraction of 0.3 m as shown in Fig 4. The retracted tube is stored as a tightly packed band in a cylinder wrapped around the base of the zipper column above the universal joint. This compact storage unit lets the arm relax against the body of the aircraft with a low profile when the arm is not in use, minimizing the effect the arm has on the maneuverability of the flyer. The zipper driver and the storage unit weigh 0.4 kg. The arm band itself weighs 0.25 kg.

The total weight of the system comes in slightly below the

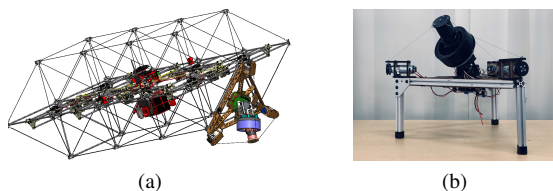


Fig. 4. A fully retracted Spiral Zipper manipulator is installed on the Propulsion Core vehicle (a) and a 80/20 frame (b) respectively.

TABLE I
MAJOR SYSTEM COMPONENT COSTS

Component	Qty	Price(\$)/Unit	Price(\$)
Nucleo-F466RE Microcontroller	1	14.90	14.90
165 RPM Gear Motor w/Encoder	4	59.99	239.96
G2 18v25 Motor Driver	4	39.95	159.80
AS5048A Rotary Sensor	2	9.34	18.68
QTR-HD-01A Reflectance Sensor	2	1.79	3.58
20' x 2" x .031" ABS Band	1	24.20	24.20
20' x 0.5" x .01" ABS Band	1	9.20	9.20
AA571 Type 221 Cyanoacrylate	1	11.56	11.56
Lazy Susan Bearing	1	37.03	37.03
Custom Zipper Friction Drive	1	30.00	30.00
Roller Bearing	5	3.30	16.5
4' x 2' x 0.25" MDF Board	1	7.74	7.74
3D Printed Components	1	25.00	25.00
Fasteners, Cables, and Wires	1	10.00	10.00
Total			608.15

target at 4.3 kg, but with more than the necessary dynamic capabilities. A serendipitous result of using these particular lightweight components is that the material cost of the system shown in Table I is also low at approximately \$600.

C. Electrical Design

Two high resolution rotary position sensors (AS5048A) are used to measure the pitch and roll angles of the tube with respect to the base. They are 14-bit resolution 0.0219 deg/LSB sensors communicating with the microcontroller over the SPI bus. The resolution of these sensors are precise enough for the intended application, and the raw sensor data is smooth enough to use them without any filters. The change in length of the tube could not be measured accurately using the number of revolutions of the tube motor due to the slippery transmission of the friction drive mechanism in the band management system. An optical quadrature phase position encoder system measures the change in length of the tube. Two alternating black and white strips shown on the body of the tube in Fig. 5a are the markers used by the encoder. There are two analog reflectance sensors placed at a specific distance from the marker strip and a comparator to convert the analog signal generated by the colored strips into a digital signal. This encoder setup can measure a change as small as 0.289 mm in the length of the tube.

For actuation, all motors are driven by simple DC motor drivers through PWM signals generated by the microcon-

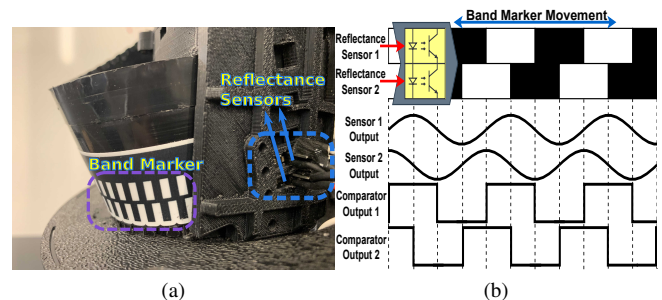


Fig. 5. (a) Band Marker with Reflectance Sensors inside the Band Management System and (b) Encoder Timing Diagram

troller. The motors have built-in quadrature encoders which are used by the microcontroller for shaft velocity feedback.

A Nucleo-F446RE microcontroller board resides on the base of the manipulator and runs the control and estimation algorithms on board. The microcontroller is able to gather quadrature phase position encoder signals from five different channels simultaneously, measure roll and pitch angles from the rotary position sensors, and drive the system's four motors.

IV. CONTROL AND ESTIMATION

A. Kinematics Model

A simulation model of this Spiral Zipper manipulator and the kinematic notation are shown in Figure 6. Three tethers and one Spiral Zipper tube are attached to our mechanical base. With respect to the whole configuration and the workspace of the robot, it is reasonable to assume that all tethers and the Spiral Zipper tube intersect at a point. The *manipulation vector*, $\mathbf{p} \in \mathbb{R}^3$, denotes the position of the end-effector relative to the base. The *attachment vector*, $\mathbf{a}_i \in \mathbb{R}^3$, represents the position vector between the tether/tube and the base, where $i = 1, 2, 3, 4$ represents joints (three tethers and one tube). The *link vector*, $\mathbf{l}_i \in \mathbb{R}^3$, denotes the vector from the position between the i th joint and the base to the end-effector which satisfies

$$\mathbf{l}_i = \mathbf{a}_i - \mathbf{p} \quad \text{for } i = 1, 2, 3, 4 \quad (1)$$

Taking the time derivative yields:

$$\mathbf{l}_i^T \dot{\mathbf{l}}_i = -(\mathbf{a}_i - \mathbf{p})^T \dot{\mathbf{p}} = (\mathbf{p} - \mathbf{a}_i)^T \dot{\mathbf{p}} \quad \text{for } i = 1, 2, 3, 4 \quad (2)$$

Eq. (2) is true for any pair of link vector and attachment vector, and stacking them together results in

$$\mathbf{B}\dot{\mathbf{l}} = \mathbf{A}\dot{\mathbf{p}} \quad (3)$$

in which

$$\mathbf{B} = \begin{bmatrix} \mathbf{l}_1^T & \mathbf{l}_2^T & \mathbf{l}_3^T & \mathbf{l}_4^T \\ \mathbf{0} & \mathbf{l}_2^T & \mathbf{0} & \mathbf{0} \\ \mathbf{0} & \mathbf{0} & \mathbf{l}_3^T & \mathbf{0} \\ \mathbf{0} & \mathbf{0} & \mathbf{0} & \mathbf{l}_4^T \end{bmatrix}_{4 \times 12} \quad \mathbf{A} = \begin{bmatrix} (\mathbf{p} - \mathbf{a}_1)^T \\ (\mathbf{p} - \mathbf{a}_2)^T \\ (\mathbf{p} - \mathbf{a}_3)^T \\ (\mathbf{p} - \mathbf{a}_4)^T \end{bmatrix}_{4 \times 3}$$

\mathbf{B} always has full rank as long as there is no zero-length link and \mathbf{A} may not have full rank. For this manipulator, this will happen when the end-effector is in the same plane with \mathbf{a}_1 , \mathbf{a}_2 and \mathbf{a}_3 which actually cannot happen due to

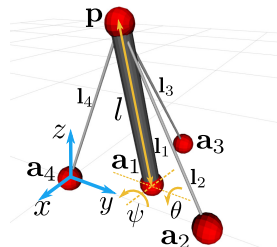


Fig. 6. Kinematics Model of Spiral Zipper Manipulator

the collision of mechanical parts. Then we can derive the following kinematics model

$$\dot{\mathbf{p}} = \mathbf{A}^+ \mathbf{B}\dot{\mathbf{l}} = \mathbf{J}\dot{\mathbf{l}} \quad (4)$$

in which \mathbf{A}^+ is the pseudo inverse of \mathbf{A} and \mathbf{J} is called the *Jacobian*. This system is overconstrained, and Eq. (4) results in the unique least square solution to Eq. (3) given $\dot{\mathbf{l}}$ is known, namely minimizing $\|\mathbf{B}\dot{\mathbf{l}} - \mathbf{A}\dot{\mathbf{p}}\|$.

B. Controller

We develop a controller to control state \mathbf{p} . The framework is shown in Fig. 7. The feedback position controller is based on resolved motion rate control [20]. The error on the state and its derivative are defined as

$$\mathbf{e} = \mathbf{p}_{\text{des}} - \mathbf{p}, \quad \dot{\mathbf{e}} = \dot{\mathbf{p}}_{\text{des}} - \dot{\mathbf{p}} \quad (5)$$

With Eq. (4) and let controller input $\mathbf{u} = \dot{\mathbf{l}}$, a continuous time system is defined

$$\dot{\mathbf{p}} = \mathbf{J}\mathbf{u} \quad (6)$$

If the error is to converge exponentially to zero, then the following equation is derived

$$\dot{\mathbf{p}}_{\text{des}} - \mathbf{J}\mathbf{u} + \mathbf{K}_p(\mathbf{p}_{\text{des}} - \mathbf{p}) = \mathbf{0} \quad (7)$$

resulting in

$$\mathbf{J}\mathbf{u} = \dot{\mathbf{p}}_{\text{des}} + \mathbf{K}_p(\mathbf{p}_{\text{des}} - \mathbf{p}) \quad (8)$$

in which \mathbf{K}_p is a positive definite gain matrix. Since this arm is an overconstrained system, the solution of \mathbf{u} is not unique. This difficulty is resolved by solving the following optimization problem

$$\begin{aligned} & \text{minimize} && \frac{1}{2} \mathbf{u}^T \mathbf{u} \\ & \text{subject to} && \mathbf{J}\mathbf{u} = \dot{\mathbf{p}}_{\text{des}} + \mathbf{K}_p(\mathbf{p}_{\text{des}} - \mathbf{p}) \end{aligned} \quad (9)$$

the solution is given by

$$\mathbf{u} = \mathbf{J}^+(\dot{\mathbf{p}}_{\text{des}} + \mathbf{K}_p(\mathbf{p}_{\text{des}} - \mathbf{p})) \quad (10)$$

where \mathbf{J}^+ is the pseudo inverse of \mathbf{J} and this is the minimum joint speed solution. Then given desired state \mathbf{p}_{des} and desired velocity $\dot{\mathbf{p}}_{\text{des}} = \dot{\mathbf{p}}_{\text{des}}$, we can compute controller input \mathbf{u} which can guarantee that the state is capable of approaching \mathbf{p}_{des} in exponential time. This control input $\mathbf{u} = [\mathbf{u}_1^T, \mathbf{u}_2^T, \mathbf{u}_3^T, \mathbf{u}_4^T]^T$ computed from Eq. (10) is the stack of desired derivative of link vector \mathbf{l}_1 , \mathbf{l}_2 , \mathbf{l}_3 and \mathbf{l}_4 .

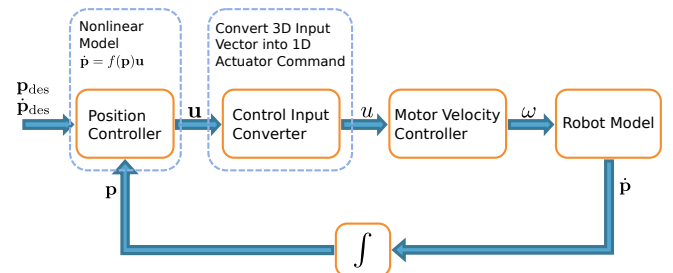


Fig. 7. The control Loop for Position Control

Given this continuous time system defined in Eq. (6) and control input \mathbf{u} , we can derive

$$\mathbf{p}(t + dt) \approx \mathbf{p}(t) + \dot{\mathbf{p}}(t)dt = \mathbf{p}(t) + \mathbf{J}(t)\mathbf{u}dt \quad (11)$$

And for each link vector \mathbf{l}_i satisfying Eq. (1),

$$d\|\mathbf{l}_i\| \approx \|\mathbf{a}_i - \mathbf{p}(t + dt)\| - \|\mathbf{a}_i - \mathbf{p}(t)\| \quad (12)$$

Each actuator of the manipulator is driven by a DC motor and $u_i \in \mathbb{R}$ where $i = 1, 2, 3, 4$ is the variable to denote how fast and in what direction the corresponding link actuator should move. u_i can be computed by

$$u_i = \begin{cases} \|\mathbf{u}_i\| & \text{if } d\|\mathbf{l}_i\| \geq 0 \\ -\|\mathbf{u}_i\| & \text{if } d\|\mathbf{l}_i\| < 0 \end{cases} \quad (13)$$

Since the system is overconstrained and it is problematic if any of the cables go slack, it is a requirement that all tethers are under tension and the Spiral Zipper tube is under compression. Hence, the Spiral Zipper tube is commanded to extend slightly faster and retract slightly slower than the computed actuator command, and the reverse is done for all tether actuators. This is applicable because tethers are elastic to some extent and tubes are very strong under compression.

Let r_i be the transmission for a link actuator, then the corresponding DC motor angular velocity is

$$\omega_i = u_i/r_i \quad (14)$$

in which $r_2 = r_3 = r_4$. Each DC motor has a quadrature encoder for angular velocity measurement, with which an angular velocity controller can be built. In the presented system, the angular velocity controller is running at 100 Hz.

C. Estimation

Two angular sensors are attached to the universal joint to measure the roll angle ψ and pitch angle θ , and the quadrature encoder signal generated from the strip on the tube is used to track the current length l of the Spiral Zipper tube as shown in Fig. 5b.

Then the manipulation vector can be derived as

$$\mathbf{p} = \mathbf{R}_{y,\theta} \mathbf{R}_{x,\psi} \begin{bmatrix} 0 \\ 0 \\ l \end{bmatrix} + \mathbf{a}_1 \quad (15)$$

in which

$$\mathbf{R}_{x,\psi} = \begin{bmatrix} 1 & 0 & 0 \\ 0 & \cos \psi & -\sin \psi \\ 0 & \sin \psi & \cos \psi \end{bmatrix}$$

$$\mathbf{R}_{y,\theta} = \begin{bmatrix} \cos \theta & 0 & \sin \theta \\ 0 & 1 & 0 \\ -\sin \theta & 0 & \cos \theta \end{bmatrix}$$

The roll angle ψ and pitch angle θ can be obtained from the rotary position sensors directly with an offset for sensor calibration. The initial length of the tube l_0 is stored in the EEPROM of the microcontroller. For each countable event, the Spiral Zipper tube moves up or down by a step Δd . The number of passed countable events N is tracked, so the length of the tube l can be computed by

$$l = \begin{cases} l_0 + N\Delta d & \text{if counter increases} \\ l_0 - N\Delta d & \text{if counter decreases} \end{cases} \quad (16)$$

V. EXPERIMENTS

We mount the Spiral Zipper arm on a frame constructed by 80/20 to test and evaluate the performance of the overall system. To show the performance of the controller, several step response experiments are performed in the x -, y - or z -axis and a VICON motion capture system is used to track the pose of the arm. \mathbf{K}_p is set to be $\text{diag}(3, 3, 1)$ and one step response result is shown in Fig. 8a which shows the manipulation vector can approach to the desired state within around 6 s in $+z$ direction. From the experiments, it is observed that the system has a faster response in x - and y -axis. This makes sense because the tether actuators have a faster response than Spiral Zipper actuator on which the response in z -axis relies the most. We then perform a trajectory following experiment. The robot is commanded to move along a quintic polynomial trajectory with zero initial and final velocity and acceleration. The desired position and velocity are updated at 20 Hz. In this experiment the arm is able to follow the commanded trajectory accurately as shown in Figure 8b with an average position error of 1.71 mm in the x -axis, 1.13 mm in the y -axis and 3.52 mm in the z -axis. For our estimator, we compare the estimated manipulation vector with the position from the VICON motion capture

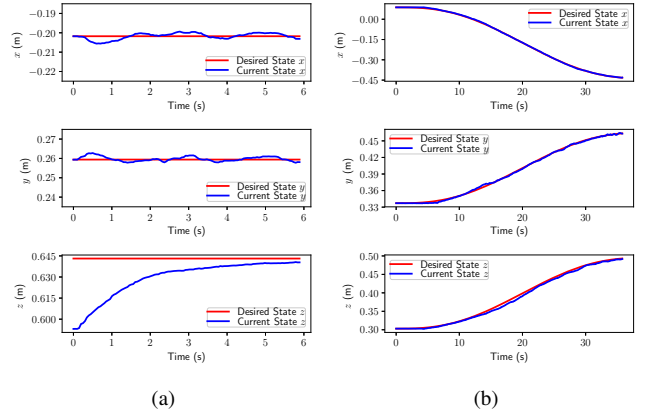


Fig. 8. (a) Step Response in $+z$ -axis and (b) Trajectory Following

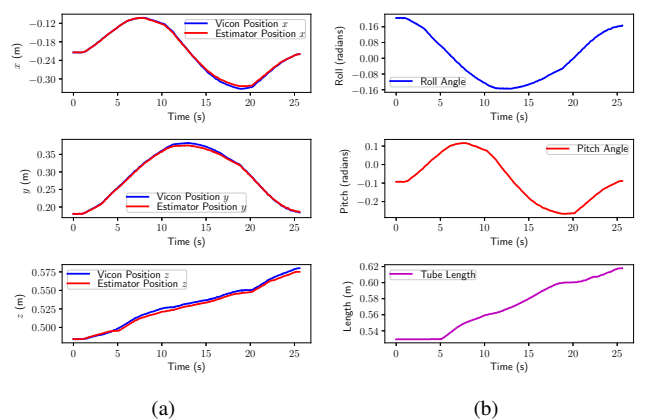


Fig. 9. Command Spiral Zipper manipulator to follow a helix trajectory.

system. The arm is commanded to follow a helix trajectory. The estimator results are accurate and shown in Fig. 9a with an average error of 2.60 mm in x -axis, 2.53 mm in y -axis and 2.96 mm in z -axis. Fig. 9b shows the data from our sensors. It is believed that much of the measured error is due to errors in the calibration of the arm's sensors relative to the accuracy of the VICON motion capture system. Another source of error is caused by the flexibility of MDF frame.

Another experiment shown in Fig. 10 is to command the manipulator to move between two positions 15 cm apart along y -axis back and forth and the command is sent at around 1.6 Hz which shows its fast dynamic response.

Finally, to simulate the aerial manipulation task, we attached a suction cup based gripper [1] to this Spiral Zipper manipulator and mounted it on the aerial vehicle frame to pick up a cellphone shown in Fig. 11. The VICON motion capture system is used to track the location of the cellphone and the manipulator approaches precisely enough so that the suction gripper can grasp the cellphone.

VI. CONCLUSIONS

This paper presents a new design of a cable driven manipulator using the Spiral Zipper prismatic joint for aerial grasping and manipulation tasks. This manipulator is designed to be low-cost and possesses a high strength to weight ratio. In addition, the manipulator has a very compact storage space relative to its workspace. The kinematics model, position controller and estimation method are developed to fully control the pose of the arm, and its performance is evaluated by some experiments. An example of an aerial grasping task is demonstrated.

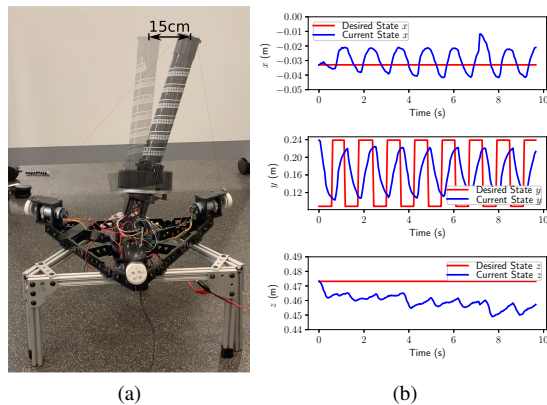


Fig. 10. Command Spiral Zipper manipulator to move between two positions by updating desired positions at around 1.6 Hz.

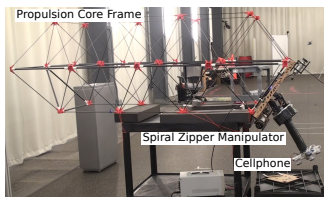


Fig. 11. Command Spiral Zipper manipulator mounted on the aerial vehicle frame to pick up a cellphone.

REFERENCES

- [1] C. C. Kessents, M. Horowitz, C. Liu, J. Dotterweich, M. Yim, and H. L. Edge, "Toward lateral aerial grasping and manipulation using scalable suction," in *2019 IEEE International Conference on Robotics and Automation (ICRA)*, May 2019.
- [2] K. Zhang, P. Chermprayong, T. M. Alhina, R. Siddall, and M. Kovac, "Spidermav: Perching and stabilizing micro aerial vehicles with bio-inspired tensile anchoring systems," in *2017 IEEE/RSJ International Conference on Intelligent Robots and Systems (IROS)*, Sep. 2017, pp. 6849–6854.
- [3] H. W. Wopereis, T. D. van der Molen, T. H. Post, S. Stramigioli, and M. Fumagalli, "Mechanism for perching on smooth surfaces using aerial impacts," in *2016 IEEE International Symposium on Safety, Security, and Rescue Robotics (SSRR)*, Oct 2016, pp. 154–159.
- [4] C. C. Kessens, J. Thomas, J. P. Desai, and V. Kumar, "Versatile aerial grasping using self-sealing suction," in *2016 IEEE International Conference on Robotics and Automation (ICRA)*, May 2016, pp. 3249–3254.
- [5] F. Collins and M. Yim, "Design of a spherical robot arm with the spiral zipper prismatic joint," in *2016 IEEE International Conference on Robotics and Automation (ICRA)*, May 2016, pp. 2137–2143.
- [6] P. E. I. Pounds, D. R. Bersak, and A. M. Dollar, "The yale aerial manipulator: Grasping in flight," in *2011 IEEE International Conference on Robotics and Automation*, May 2011, pp. 2974–2975.
- [7] D. Mellinger, Q. Lindsey, M. Shomin, and V. Kumar, "Design, modeling, estimation and control for aerial grasping and manipulation," in *2011 IEEE/RSJ International Conference on Intelligent Robots and Systems*, Sep. 2011, pp. 2668–2673.
- [8] J. DeGol, D. Hanley, N. Aghasadeghi, and T. Bretl, "A passive mechanism for relocating payloads with a quadrotor," in *2015 IEEE/RSJ International Conference on Intelligent Robots and Systems (IROS)*, Sep. 2015, pp. 4337–4342.
- [9] M. Orsag, C. Korpela, and P. Oh, "Modeling and control of mm-uav: Mobile manipulating unmanned aerial vehicle," *Journal of Intelligent & Robotic Systems*, vol. 69, no. 1, pp. 227–240, Jan 2013.
- [10] T. W. Danko and P. Y. Oh, "A hyper-redundant manipulator for mobile manipulating unmanned aerial vehicles," in *2013 International Conference on Unmanned Aircraft Systems (ICUAS)*, May 2013, pp. 974–981.
- [11] R. Cano, C. Perez, F. Pruaño, A. Ollero, and G. Heredia, "Mechanical design of a 6-dof aerial manipulator for assembling bar structures using uavs," in *Proc. 2nd RED-UAS Workshop Res., Education Develop. Unmanned Aerial Syst.*, Nov. 2013.
- [12] M. Orsag, C. Korpela, S. Bogdan, and P. Oh, "Valve turning using a dual-arm aerial manipulator," in *2014 International Conference on Unmanned Aircraft Systems (ICUAS)*, May 2014, pp. 836–841.
- [13] C. D. Bellicoso, L. R. Buonocore, V. Lippiello, and B. Siciliano, "Design, modeling and control of a 5-dof light-weight robot arm for aerial manipulation," in *2015 23rd Mediterranean Conference on Control and Automation (MED)*, June 2015, pp. 853–858.
- [14] A. Suarez, G. Heredia, and A. Ollero, "Lightweight compliant arm for aerial manipulation," in *2015 IEEE/RSJ International Conference on Intelligent Robots and Systems (IROS)*, Sep. 2015, pp. 1627–1632.
- [15] A. E. Jimenez-Cano, G. Heredia, and A. Ollero, "Aerial manipulator with a compliant arm for bridge inspection," in *2017 International Conference on Unmanned Aircraft Systems (ICUAS)*, June 2017, pp. 1217–1222.
- [16] A. Q. L. Keemink, M. Fumagalli, S. Stramigioli, and R. Carloni, "Mechanical design of a manipulation system for unmanned aerial vehicles," in *2012 IEEE International Conference on Robotics and Automation*, May 2012, pp. 3147–3152.
- [17] T. W. Danko, K. P. Chaney, and P. Y. Oh, "A parallel manipulator for mobile manipulating uavs," in *2015 IEEE International Conference on Technologies for Practical Robot Applications (TePRA)*, May 2015, pp. 1–6.
- [18] M. Kamel, K. Alexis, and R. Siegwart, "Design and modeling of dexterous aerial manipulator," in *2016 IEEE/RSJ International Conference on Intelligent Robots and Systems (IROS)*, Oct 2016, pp. 4870–4876.
- [19] M. Fumagalli, S. Stramigioli, and R. Carloni, "Mechatronic design of a robotic manipulator for unmanned aerial vehicles," in *2016 IEEE/RSJ International Conference on Intelligent Robots and Systems (IROS)*, Oct 2016, pp. 4843–4848.
- [20] D. E. Whitney, "Resolved motion rate control of manipulators and human prostheses," *IEEE Transactions on Man-Machine Systems*, vol. 10, no. 2, pp. 47–53, June 1969.